

Deformation and fracture of mica-containing glass-ceramics in Hertzian contacts

Hongda Cai,^{a)} Marion A. Stevens Kalceff,^{b)} and Brian R. Lawn

Materials Science and Engineering Laboratory, National Institute of Standards and Technology, Gaithersburg, Maryland 20899-0001

(Received 2 August 1993; accepted 29 October 1993)

The Hertzian indentation response of a machinable mica-containing glass-ceramic is studied. Relative to the highly brittle base glass from which it is formed, the glass-ceramic shows evidence of considerable "ductility" in its indentation stress-strain response. Section views through the indentation sites reveal a transition from classical cone fracture outside the contact area in the base glass to accumulated subsurface deformation-microfracture in the glass-ceramic. The deformation is attributed to shear-driven sliding at the weak interfaces between the mica flakes and glass matrix. Extensile microcracks initiate at the shear-fault interfaces and propagate into the matrix, ultimately coalescing with neighbors at adjacent mica flakes to effect easy material removal. The faults are subject to strong compressive stresses in the Hertzian field, suggesting that frictional tractions are an important element in the micromechanics. Bend-test measurements on indented specimens show that the glass-ceramic, although weaker than its base glass counterpart, has superior resistance to strength degradation at high contact loads. Implications of the results in relation to microstructural design of glass-ceramics for optimal toughness, strength, and wear and fatigue properties are discussed.

I. INTRODUCTION

Hertzian indentation of homogeneous brittle materials, such as glasses and single crystals, has received extensive attention in the literature.¹⁻²⁰ Above a critical load, a ring crack initiates in the weakly tensile region just outside the circle of contact with the indenting sphere, propagates downward as a surface-truncated cone, and finally arrests at a depth approximately equal to the contact radius.^{6,15} This is the so-called Hertzian cone crack.²¹ Hertzian fracture is of interest to materials scientists for its uncommon insight into the stability of strength-degrading flaws^{6,20} and for its intrinsic relation to material toughness.^{6,15}

Few Hertzian indentation studies have been made of the newer generation of tougher polycrystalline and two-phase ceramics, where microstructure plays a critical role in the fracture behavior. Some cone fracture observations have previously been reported on low-toughness fine-grain monophase ceramics^{15,22} and brittle lithium-silicate glass-ceramics.^{23,24} Higher long-crack fracture toughness occurs in those ceramics with larger grains and greater internal mismatch stresses^{25,26} and is attributable most commonly to crack-interface "bridging" from interlock-

ing grains or particles.^{20,27-31} Recently, examination of Hertzian indentations in a coarse-grain polycrystalline alumina³² has revealed a radical departure from the classical fracture pattern; the cone crack is suppressed in favor of distributed damage in a zone of high compression-shear beneath the contact circle, more reminiscent of deformable solids. The subsurface damage takes the form of deformation-microfracture by precursor intragrain twin/slip and subsequent grain-localized intergranular microfracture. Repeat loading exacerbates the extent of the subsurface damage, leading to microcrack coalescence and ultimately surface removal.³² The transition from cone fracture to accumulated damage zone occurs above a threshold grain size, indicating a microstructural scaling effect.³³ Thus, the same microstructural elements responsible for the enhanced toughness properties change the entire nature of the fracture damage process.

One class of ceramics that has received considerable attention for use as model two-phase systems as well as in practical applications is glass-ceramics.³⁴ A system of particular interest is that of a glass matrix containing crystallized mica platelets, the size and density of which may be readily controlled by simple heat treatments.³⁵⁻³⁷ Mica-containing glass-ceramics are best known for their easy machinability,³⁷⁻³⁹ an attractive quality for forming operations used in dental restorations⁴⁰ and other applications. Yet these same glass-ceramics have

^{a)}Guest Scientist on leave from Department of Materials Science and Engineering, Lehigh University, Bethlehem, Pennsylvania 18015.

^{b)}Guest Scientist on leave from Department of Applied Physics, University of Technology, Sydney, New South Wales 2007, Australia.

respectable long-crack toughness.^{37,39,41} Such countervailing responses in the short-crack and long-crack regions raise questions as to the role of the mica-matrix microstructure in the micromechanisms of deformation and fracture.

In this paper we study the Hertzian indentation response of one mica-containing machinable glass-ceramic, "Macor", using comparison tests on the precursor "green" glass to establish a baseline brittle state. We will show that in the Macor, as in coarse-grain alumina, well-defined cone fracture is supplanted by accumulated subsurface deformation-microfracture damage. This transition is quantified on an indentation stress-strain curve. The deformation takes the form of shear faulting along weak mica-glass interfaces. Microcracks extend from the ends of these faults into the glass matrix, and ultimately coalesce with their neighbors to effect material fragmentation and removal. The shape of the macroscopic damage zone is discussed in relation to the distribution of shear stresses beneath the contact area, with due allowance for sliding friction tractions at the compressively closed faults. Strength degradation associated with the damage is measured as a function of indentation load for both the crystallized and green Macor, and is discussed in terms of the relative toughness properties.

II. EXPERIMENTAL

The material used in this study was a commercial mica-containing glass-ceramic, produced under the trade name Macor (Corning Inc., Corning, NY). Macor composition in weight % is 46% SiO₂, 14% MgO, 16% Al₂O₃, 10% K₂O, 8% B₂O₃, and 6% F). In its final heat-treated form, Macor exists in a partially crystallized state, with composition ≈55% fluorophlogopite mica and ≈45% borosilicate glass. Specifically, the microstructure consists of a network of randomly oriented interlocking mica flakes.³⁵⁻³⁸ The individual flakes are approximately 10 μm in surface dimension parallel to the cleavage basal plane, and 1 to 2 μm thick normal to this plane. Simplistically, the network of closely packed planes of weakness, i.e., mica basal cleavage and mica-glass interfaces, facilitates easy fracture in the short-crack domain, thereby accounting for the machinability.³⁵ At the same time, once a crack develops over a scale large relative to the microstructure the mica flakes act as effective bridges across the separation plane, giving rise to a progressively rising toughness curve and enhancing the long-crack toughness.⁴¹

The "green" glass from which the final crystallized form of Macor is derived was used as a reference material for baseline comparison. This base glass has an opalescent white color, due to the presence of submicrometer-scale fluorine-rich droplets from liq-

uid phase separation during the original glass-forming process.³⁵ The droplets comprise nucleation centers for the ultimate formation of mica phases in the crystallization heat treatments.³⁵⁻³⁷

Plate specimens 25 mm square and 4 mm thick were cut from billets of mica-containing Macor and base glass. Surfaces for indentation stress-strain testing were polished with diamond paste to 1 μm finish, and then coated with gold. Indentations were made using tungsten carbide spheres of radii $r = 0.79, 1.19, 1.98, 3.18, 4.76, 7.94, \text{ and } 12.70$ mm, over a load range $P = 0$ to 2000 N using a universal testing machine (Instron Model 1122, Instron Corp., Canton, MA). Residual traces in the gold layer enabled determinations of contact radius a at each applied load,³² and thence contact pressure ($p_0 = P/\pi a^2$) as a function of indentation strain (a/r) (see Sec. III).

For detailed microscopic investigation of the subsurface damage, a special bonded-interface specimen configuration was employed,³³ following a procedure first described by Mulhearn.⁴² In this configuration, shown in Fig. 1, two half-specimens with polished surfaces were clamped together with a thin layer (≈1 μm) of a cyanoacrylate-based adhesive (SuperBonder, Locite Corp., Newington, CT) to form a bonded interface. The

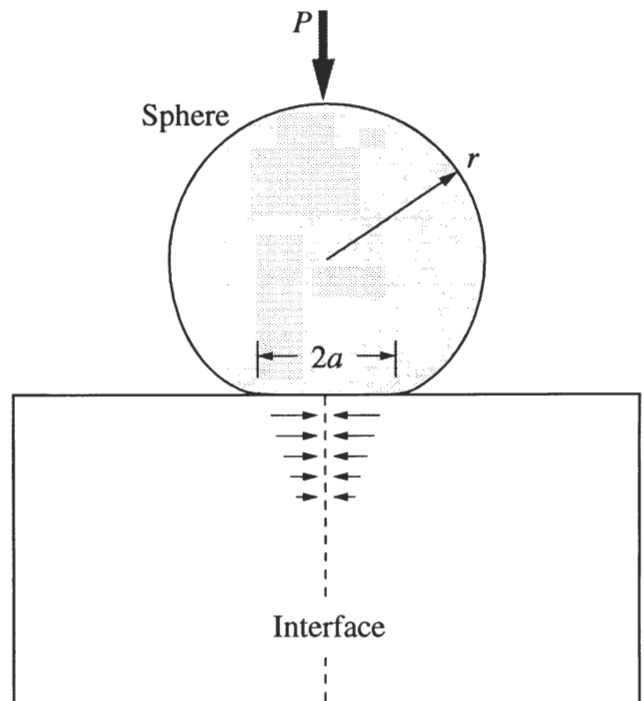


FIG. 1. Hertzian test geometry for bonded-interface specimen. Sphere, radius r , delivers load P over contact radius a . Specimen consists of two polished halves bonded across the interface. Compressive stresses beneath contact (arrows) and from external clamping (not shown) maintain contact between specimen halves during indentation.

ultimate indentation test surface was then ground and polished perpendicular to the bonded interface. A sequence of indentations was subsequently made along the interface trace at the test surface, taking special care to keep the contacts centered across this trace. It was found beneficial to apply a clamping stress normal to the interface during indentation to minimize intersurface separation. After indentation, the interface specimens were soaked in acetone to dissolve the adhesive and to separate the specimens into their two halves. After cleaning the surfaces, reflection optical microscopy in Nomarski interference contrast was used to examine the subsurface deformation and fracture patterns in section view.

Some Vickers indentations were made to measure the hardness of the base glass and the mica-containing glass-ceramic.

Bars $48 \times 6 \times 4$ mm were machined for measurement of strength degradation from Hertzian contact damage. The prospective test faces and sides of these bars were polished to $3 \mu\text{m}$ finish. All specimens were chamfered at their edges and acid-etched in 2% HF solution for 15 min to minimize edge failures in the ensuing strength tests. The strength tests themselves were conducted in four-point bending. An indentation was made at the center of each polished surface at a specified contact load, using a sphere of radius 3.18 mm at a loading/unloading rate $100 \text{ N} \cdot \text{s}^{-1}$. At low loads in the base glass, multiple indentations were made in order to ensure the most favorable conditions for cone fracture. Some specimens were left unindented to measure "natural" strengths.⁴³ A drop of silicone oil was placed on the indentation sites prior to flexure, and the tests conducted in rapid loading (<50 ms failure time) to minimize effects of slow crack growth from environmental moisture. Broken specimens were examined to ensure that the fracture originated from the indentation sites. Those that did not were included in the data pool for unindented specimens because fracture originated from "natural" flaws in those specimens.

III. RESULTS

A. Indentation stress-strain curves

Indentation stress-strain data for the Macor mica-containing glass ceramic and the base glass are shown in Fig. 2. The responses were obtained by monitoring mean contact pressure

$$p_0 = P/\pi a^2 \quad (1)$$

as a function of the geometrical ratio a/r , with P the indentation load, a the radius of contact, and r the sphere radius. The data for each material fall on a universal curve, independent of r , consistent with the principle of geometrical similarity.^{10,16,44} In the low-strain elastic

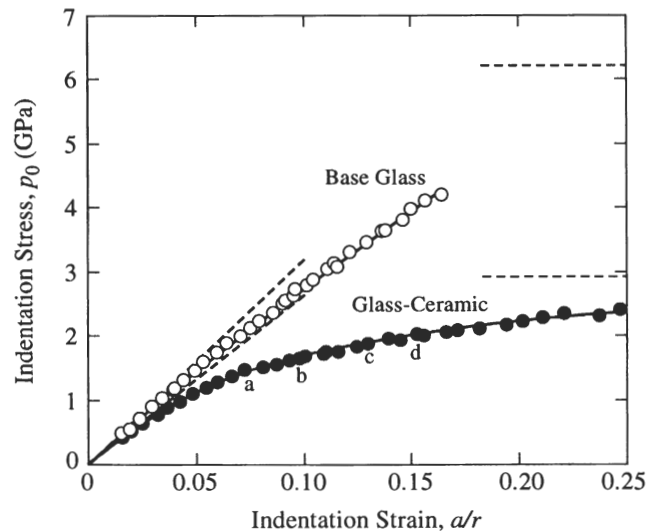


FIG. 2. Indentation stress-strain curves for Macor mica-containing glass-ceramic and base glass, using WC spheres of radii $r = 0.79, 1.19, 1.98, 3.18, 4.76, 7.94,$ and 12.70 mm (not distinguished on data points). Solid curves are empirical fits to the data. Inclined dashed lines are Hertzian elastic responses computed from Eq. (2) using Young's modulus from independent ultrasonic measurement and Poisson's ratio from manufacturer's specifications as follows: $E_S = 614$ GPa and $\nu_S = 0.22$ for WC spheres; $E = 77$ GPa and $\nu = 0.29$ for base glass (upper dashed line); and $E = 63$ GPa and $\nu = 0.29$ for Macor (lower dashed line). Horizontal dashed lines indicate Vickers hardness for base glass (upper) and Macor (lower). Points *a*, *b*, *c*, and *d* on Macor curve correspond to pressures used later in sequence in Fig. 4.

region prior to irreversible deformation, the data lie close to the inclined dashed lines representing the classical Hertzian relation^{20,45}:

$$p_0 = (3E/4\pi k)(a/r), \quad (2)$$

where E is Young's modulus of the specimen material; $k = (9/16)[(1 - \nu^2) + (1 - \nu_S^2)(E/E_S)]$ is a dimensionless constant of each indenter/specimen combination, with ν Poisson's ratio and subscript S designating the sphere material. Young's moduli used in our evaluations of Eq. (2) were determined from independent ultrasonic measurements on the Macor and base glass, and are included in the caption to Fig. 2. In the high-strain region the data approach the hardness values from the Vickers tests.

We note the clear distinction in stress-strain response between the crystallized Macor and precursor base glass. The base glass behaves in an ideal brittle manner, with near-linear response over the data range. By contrast, the mica-containing Macor deviates dramatically from the linear response at a relatively low indentation stress. It is evident that crystallization of the mica phase has conferred a degree of "plasticity" to the glass-ceramic, more like a ductile metal than a brittle ceramic.

B. Microscopic observations of subsurface damage

Half-surface and side views of Hertzian indentations in the base glass are shown in Fig. 3. Classical concentric cone cracks^{4,6,15,46,47} are observed. The contact radius at maximum pressure lies just within the outermost surface ring in Fig. 3, confirming that the cone fractures form in the region of weak tension outside the subsurface compression-shear zone.¹⁵ Note that there is no detectable deformation beneath the contact circle; essentially, the material behaves as an ideally homogeneous solid.

Analogous half-surface and side views for the mica-containing glass-ceramic are shown in Fig. 4, as a sequence of increasing indentation pressures. In these micrographs the mica flakes in the glass matrix are readily observable in the Nomarski illumination. Cone fracture outside the contact area is now inactive. Instead, the indentation takes on the appearance of a "plastic" impression, reminiscent of the subsurface plasticity zone beneath contacts in ductile metals.⁴² The evolution of the damage is most clearly revealed in the section views. In Fig. 4(a), the damage starts subsurface and gradually

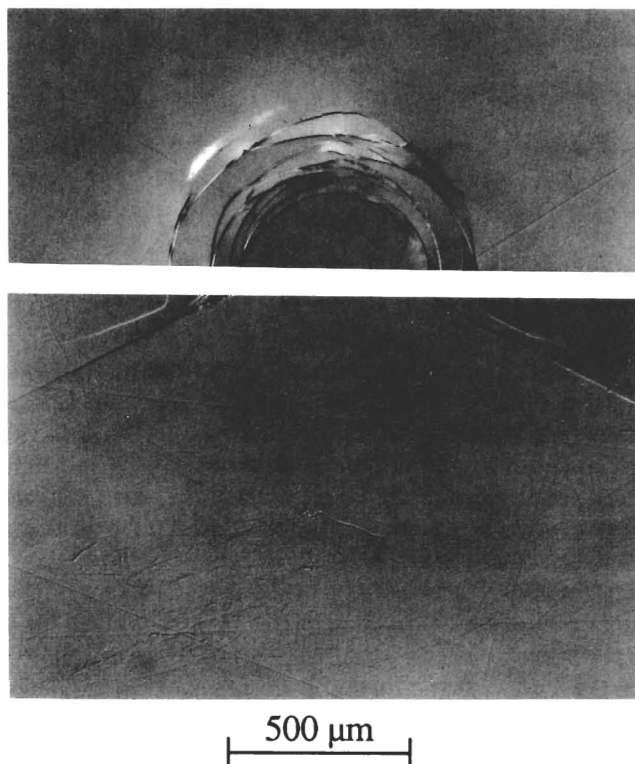


FIG. 3. Optical micrographs of indented base glass, showing half-surface (top) and section (bottom) views of Hertzian cone fracture in bonded-interface specimen, WC sphere radius $r = 3.18$ mm at contact pressure $p_0 = 2.88$ GPa, corresponding to contact radius $a = 330$ μm at load $P = 1000$ N. Viewed in Nomarski interference illumination.

progresses in Figs. 4(b) and 4(c) to the surface until, in Fig. 4(d), the "plastic zone" is fully developed. Note that there is a near-surface region immediately below the contact area where damage appears to be suppressed, even in the more advanced stages of impression in Figs. 4(c) and 4(d).

Higher magnification views of the subsurface damage zones in Fig. 5 reveal interrelations between the damage process and the mica plate structure more clearly. The micrograph in Fig. 5(a) is from a region of relatively low damage, point A in Fig. 4(c). Discrete microcracks appear along the interfaces between glass matrix and mica plates. The micrograph in Fig. 5(b) is from a region of higher damage, point B in Fig. 4(d). It shows microcracks extending from individual mica plates into the glass matrix and linking up with neighbors to form coalesced fracture arrays. No microcracking was observed outside the damage zone.

C. Strength degradation

Results from the Hertzian-indentation/inert-strength tests for the Macor mica-containing glass ceramic and the base glass are plotted in Fig. 6. In this diagram the error bars are standard deviations for an average of 4 specimens per data point. The hatched boxes at left indicate strengths of specimens that broke away from indentation sites. Solid curves are empirical fits to the data.¹⁸

The curves in Fig. 6 show some interesting contrasts, not least the fact that they cross each other. For the Macor glass-ceramic, the strength shows a steady decline with load above the cutoff strength level for failures from natural flaws. This response is characteristic of materials with a low damage threshold but moderate toughness. For the base glass, the strength maintains its high value for natural surfaces up to the critical indentation load for cone fracture, above which it drops precipitously and thereafter declines with increasing load. This response is characteristic of materials with a high damage threshold but low toughness. Thus, although the Macor in its crystallized form may appear to have inferior laboratory strength relative to its base glass counterpart, its ultimate resistance to strength loss from sustained damage is markedly superior, except perhaps at extreme high loads.

IV. DISCUSSION

We have demonstrated that Macor, a mica-containing machinable glass-ceramic, undergoes extensive irreversible damage under Hertzian indentations. The nature of the damage is radically different from the classical cone fracture that forms outside the contact circle in brittle glasses and single crystals. Macroscopically, the damage pattern resembles the form of the continuous plastic zones that form in the subsurface slip-line fields beneath indentations in ductile metals.⁴² One may

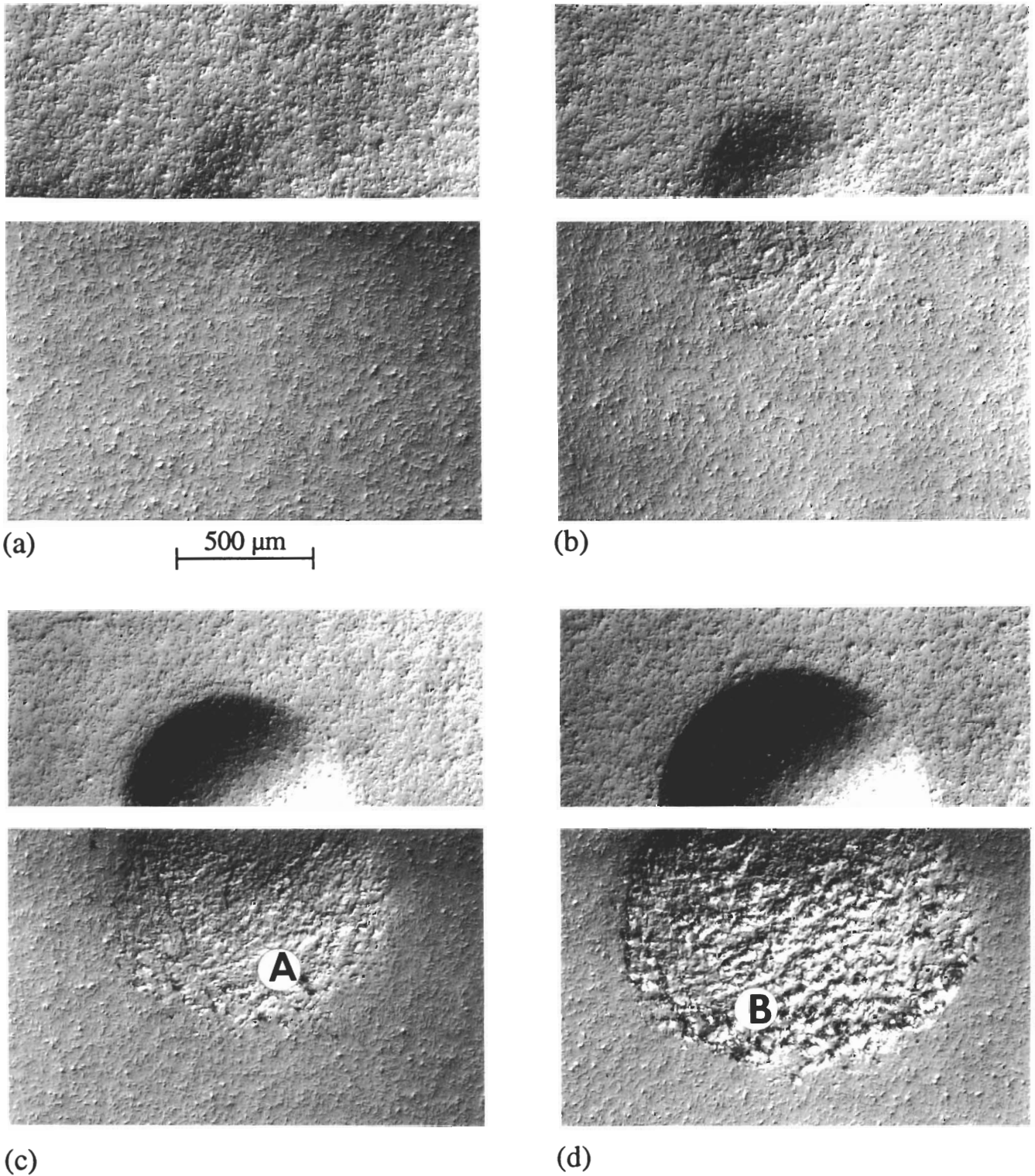
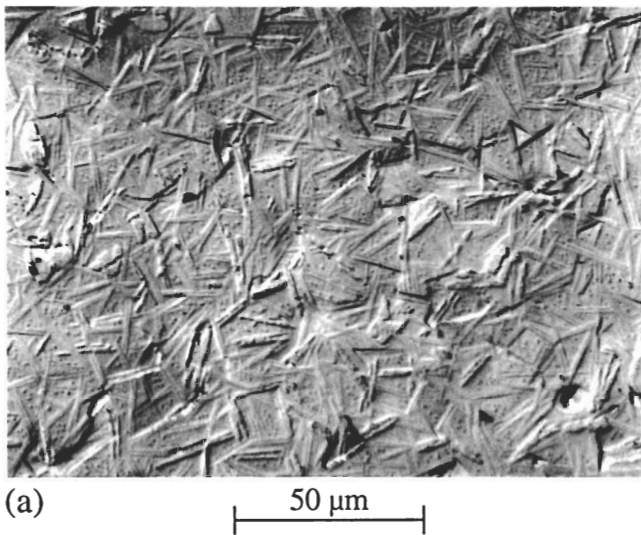
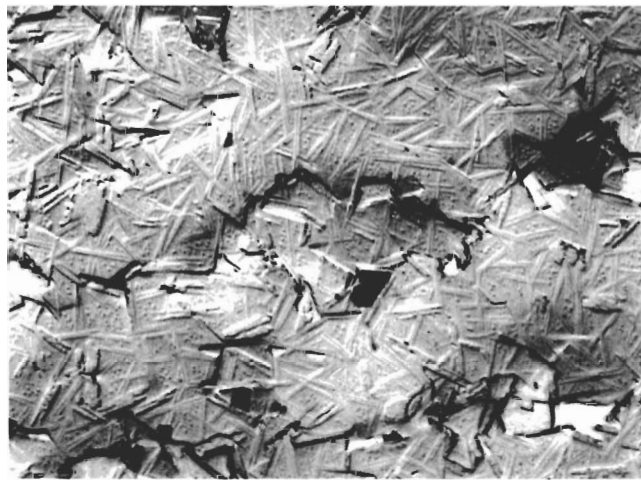


FIG. 4. Optical micrographs of indented Macor glass-ceramic, showing half-surface (top) and section (bottom) views of subsurface deformation-microfracture damage evolution in bonded-interface specimens, at indentation stress (a) $p_0 = 1.46$ GPa, (b) 1.63 GPa, (c) 1.87 GPa, and (d) 2.02 GPa. The corresponding indentation loads are $P = 250, 500, 1000,$ and 1500 N. WC sphere radius $r = 3.18$ mm. Viewed in Nomarski interference illumination. Locations A in (c) and B in (d) expanded in Fig. 5.

accordingly regard the observed change in indentation response in the glass-ceramic as akin to a brittle-ductile transition, although the deformation micromechanism

differs fundamentally from the traditional dislocation flow process. Microscopically, the damage bears a strong resemblance to the discrete microslip-microfracture

(a) 50 μm 

(b)

FIG. 5. Enlarged optical micrographs showing subsurface damage in Macor glass-ceramic showing microcracks: (a) individual microcracks at mica-glass interfaces in low damage area [location A in Fig. 4(c)]; and (b) coalesced microcracks in high damage area [location B in Fig. 4(d)]. Viewed in Nomarski interference illumination.

patterns observed in rocks subjected to confining pressures.⁴⁸⁻⁵¹ Similar discreteness in subsurface damage patterns has also been reported in zinc sulfide polycrystals⁵² beneath Vickers hardness impressions.

The indentation stress-strain curve in Fig. 2 is a simple methodology for quantifying the deformation response. In particular, the extreme nonlinear curve in the glass-ceramic is a graphic measure of the "ductility" that results from the crystallization process. It also allows for specification of such useful material parameters as "yield stress"⁴⁴ not otherwise accessible by conventional tensile testing routines used to determine mechanical responses of highly brittle solids.

The bonded-interface indentation experiment used in Figs. 3 and 4 is particularly effective for revealing

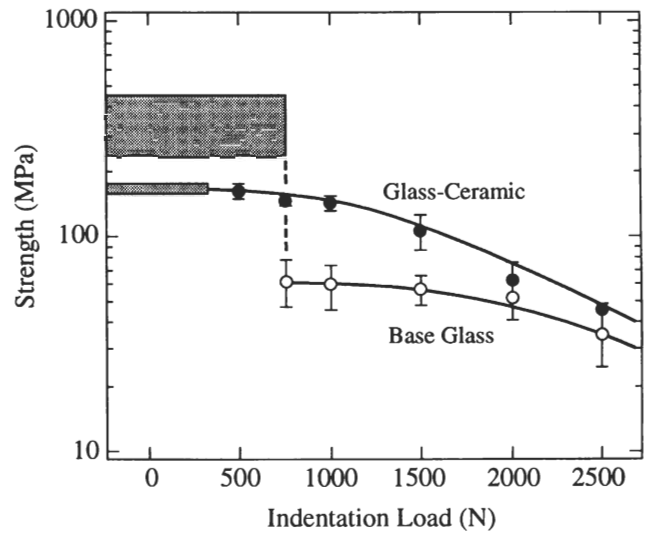


FIG. 6. Inert strength of Macor mica-containing glass-ceramic and base glass after indentation with WC sphere, radius $r = 3.18$ mm, as a function of indentation load. Solid curves are empirical curve fits. Note that curves cross each other. Shaded regions at left represent standard deviation limits for all breaks away from indentation sites. Vertical dashed line for base glass data indicates approximate threshold load for cone crack formation.

the subsurface damage. This effectiveness is attributable to the detectability of very small (nanometer-scale) shear offsets at the separated free surfaces by Nomarski interference contrast. Polished sections are much less informative, because the very act of polishing removes these offsets. Indeed, polishing away less than $1 \mu\text{m}$ of the newly separated surfaces is sufficient to render much of the detail in Figs. 3 and 4 invisible. It is acknowledged that the presence of the interface in the experimental configuration of Fig. 1 could influence the observations, by relaxing the stresses on the median plane. However, Mulhearn's earlier definitive studies found no such relaxation effect in metals.⁴² Moreover, the damage occurs in the immediate subsurface zone where the opposing surfaces are maintained in mutual contact by compressive stresses (arrows in Fig. 1). In some of our initial experiments certain artifacts (e.g., detachment of the material within the deformation zone) were indeed observed if the specimen was not constrained, especially at higher indentation loads; however, this problem could be avoided by applying clamping stresses as described in Sec. II.

The explicit nature of the deformation mechanism in the mica-containing glass-ceramic is not completely resolved in our observations, but most certainly involves some kind of discrete shear faulting of the weak interfaces.³⁵ Again, the rock mechanics literature provides rich precedent for the existence of such shear failures.⁴⁸⁻⁵¹ Individual microcracks develop at these interfaces on loading and unloading the indenter

[Fig. 5(a)], and ultimately coalesce to form shear-damage bands [Fig. 5(b)]. The microcracking appears to occur along the mica-glass interface rather than along the low-energy cleavage plane of mica, suggesting that the mica cleavage planes are stronger than the mica-glass interfaces. We note that the mica flakes in the subsurface deformation zone are not exposed to the external environment [at least not until the damage bands in Fig. 5(b) intersect the surface], and that the cleavage energy of mica remains relatively high unless exposed to moisture ($>2000 \text{ mJ} \cdot \text{m}^{-1/2}$ in "dry" environments vs $\approx 500 \text{ mJ} \cdot \text{m}^{-1/2}$ in laboratory air⁵³⁻⁵⁵). High thermal expansion mismatch stresses may augment the interfacial microcracking³⁵; such augmented microcracking has indeed been observed at Hertzian contacts in composites of silicon carbide particles in glass matrices, where the mismatch stresses are enhanced by adjusting the glass composition.²⁶

The notion of shear faulting at the weak mica-glass interfaces is consistent with the shape of the deformation zone in the Hertzian stress field. Compression stresses act normal to the fault planes,³² thereby maintaining the sliding surfaces in intimate contact during the indentation process. Friction must, therefore, be a key element of the micromechanical description. Accordingly, we may write the *net* shear stress S on a mica-glass interface in the generic form:

$$S = |\tau_F| - \mu|\sigma_F| \quad (3)$$

where τ_F and σ_F are the local shear and compressive stresses on the fault plane and μ is the coefficient of sliding friction. The condition for sliding is that $S > 0$, so subzero values of S are inadmissible in Eq. (3).^{48,49,51,56} Contours of S for faults oriented for maximum local shear at each point within the Hertzian field⁴⁵ are plotted in Fig. 7 for specified values of μ and a Poisson's ratio $\nu = 0.29$ for the glass-ceramic. These contours appear to reflect the broad geometrical features of the evolving deformation zone in Fig. 4. Note the development of a near-surface domain (shaded) within which S is effectively zero, corresponding to faults for which the closure stress is so high as to preclude any sliding in Eq. (3). This zone increases with friction coefficient until, at $\mu = 1$, it occupies virtually the entire subsurface region. Such a zone of zero net shear stress is consistent with the observations of a region of suppressed damage immediately below the contacts in Fig. 4.

The manner in which microcracks extend in extensile mode from the edges of the faults and eventually link up is a complex problem in damage mechanics. Once more, interfacial friction must play a pivotal role in any fracture mechanics model.^{56,57} A generic treatment of this problem in the special context of Hertzian contacts will be presented elsewhere.⁵⁸

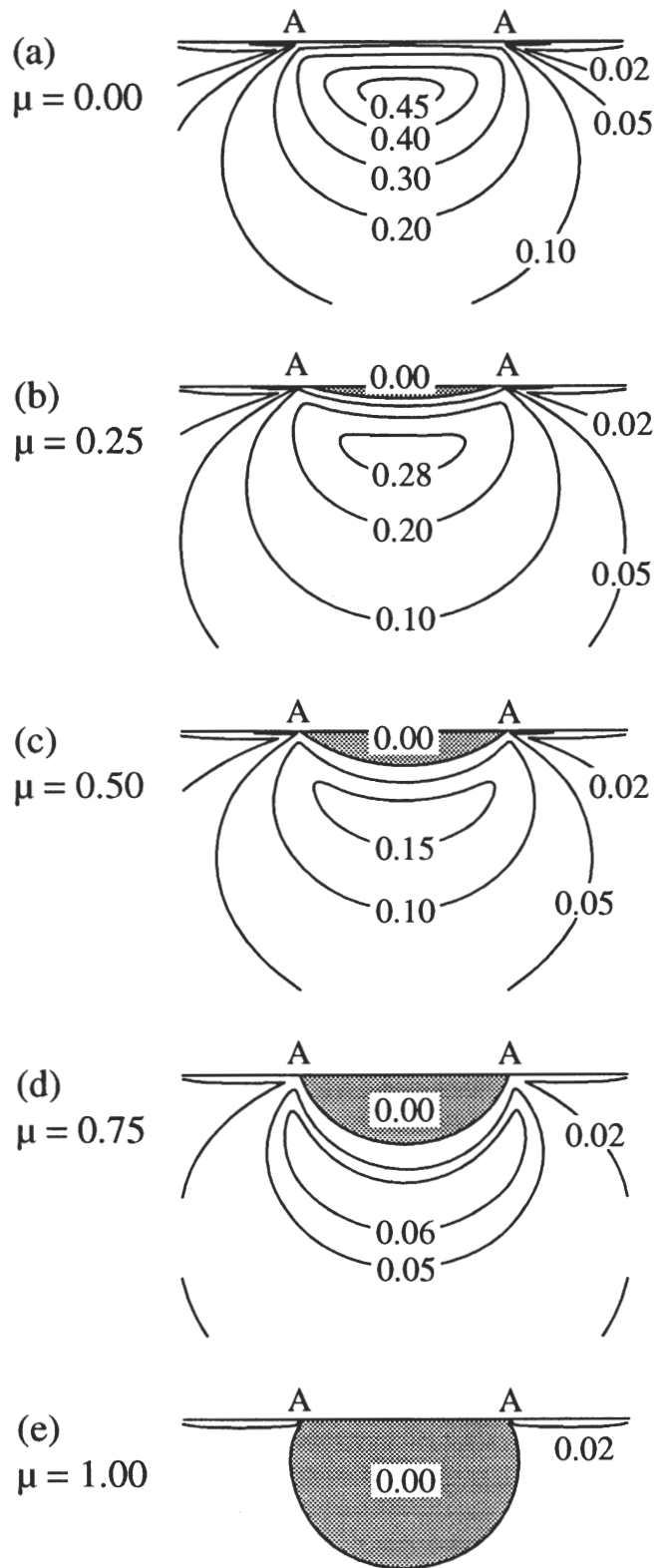


FIG. 7. (a-e) Contours of net shear stress S within Hertzian field for different friction coefficients μ in Eq. (3) and for Poisson's ratio 0.29 for Macor. Note strong suppression in stress levels as μ increases.

The results presented here bear on a broad range of mechanical properties, particularly in relation to the issue of toughness-curve behavior.²⁰ We commented on the interrelation between contact damage and strength in Sec. III. C. The data in Fig. 6 demonstrate that a material with relatively low laboratory strength (due to the presence of weak mica-glass interfaces as in this case of crystallized Macor) may nevertheless be more immune to degrading contact damage in service conditions. Although relative to the base glass the Macor has a lower short-crack toughness, it also has greater long-crack toughness; the toughness-curves for the Macor and the base glass cross each other.^{41,59,60} As we have already mentioned, it is this relative weakness in the short-crack domain that accounts for the machinability of the Macor. Accordingly, following the experience with coarse-grain aluminas,^{32,33} we may expect the crystallized Macor to have an entirely different fatigue response to that of the base glass.⁶¹ It is most likely that, under cyclic fatigue loading, the microcrack faces slide and wear against each other, resulting in frictional attrition⁶² and thereby causing microcracks to extend and ultimately coalesce.

Finally, there are strong implications in the present work concerning the microstructural design of materials systems for optimal mechanical properties. In the case of glass-ceramics the deformation and fracture responses can be altered through the controlled crystallization of a second phase in the glass matrix by heat treatment. The optimum treatment for a specific application will inevitably depend on an appropriate balance between the countervailing requirements of long-crack toughness, intermediate-crack strength, and short-crack wear and fatigue resistance.

ACKNOWLEDGMENTS

The authors thank F. Guiberteau and N. P. Padture for fruitful discussions, B. M. Hooks and M. Hill for experimental assistance, and K. Chyung of Corning Inc. for supplying the mica-containing Macor and "green" Macor materials for this study. Funding was provided by the United States Office of Naval Research.

REFERENCES

1. V. R. Howes and S. Tolansky, Proc. R. Soc. London A **230**, 287–293 (1955).
2. V. R. Howes and S. Tolansky, Proc. R. Soc. London A **230**, 294–301 (1955).
3. J. P. Tillet, Proc. Phys. Soc. London B **69**, 47–54 (1956).
4. F. C. Roesler, Proc. Phys. Soc. London B **69**, 981 (1956).
5. B. R. Lawn and H. Komatsu, Philos. Mag. **14**, 689–699 (1966).
6. F. C. Frank and B. R. Lawn, Proc. R. Soc. London A **299**, 291–306 (1967).
7. B. R. Lawn, J. Appl. Phys. **39**, 4828–4836 (1968).
8. F. B. Langitan and B. R. Lawn, J. Appl. Phys. **40**, 4009–4017 (1969).
9. F. B. Langitan and B. R. Lawn, J. Appl. Phys. **41**, 3357–3365 (1970).
10. M. V. Swain and B. R. Lawn, Phys. Status Solidi **35**, 909–923 (1969).
11. A. G. Mikosza and B. R. Lawn, J. Appl. Phys. **42**, 5540–5545 (1971).
12. T. R. Wilshaw, J. Phys. D: Appl. Phys. **4**, 1567–1581 (1971).
13. J. S. Nadeau, J. Am. Ceram. Soc. **56**, 467–472 (1973).
14. M. V. Swain, J. S. Williams, B. R. Lawn, and J. J. H. Beek, J. Mater. Sci. **8**, 1153–1164 (1973).
15. B. R. Lawn and T. R. Wilshaw, J. Mater. Sci. **10**, 1049–1081 (1975).
16. M. V. Swain and J. T. Hagan, J. Phys. D: Appl. Phys. **9**, 2201–2214 (1976).
17. A. G. Evans and T. R. Wilshaw, Acta Metall. **24**, 939–956 (1976).
18. B. R. Lawn and D. B. Marshall, in *Fracture Mechanics of Ceramics*, edited by R. C. Bradt, D. P. H. Hasselman, and F. F. Lange (Plenum, New York, 1978), Vol. 3, pp. 205–229.
19. R. Warren, Acta Metall. **26**, 1759–1769 (1978).
20. B. R. Lawn, *Fracture of Brittle Solids* (Cambridge University Press, Cambridge, 1993).
21. H. Hertz, *Hertz's Miscellaneous Papers*, Chaps. 5 and 6 (Macmillan, London, 1896).
22. K. Zeng, K. Breder, and D. J. Rowcliffe, Acta Metall. **40**, 2601–2605 (1992).
23. J. S. Nadeau and A. S. Rao, J. Can. Ceram. Soc. **41**, 63–67 (1972).
24. B. R. Lawn, T. R. Wilshaw, T. I. Barry, and R. Morrell, J. Mater. Sci. **10**, 179–182 (1975).
25. P. Chantikul, S. J. Bennison, and B. R. Lawn, J. Am. Ceram. Soc. **73**, 2419–2427 (1990).
26. H. Cai, N. P. Padture, B. M. Hooks, and B. R. Lawn, J. European Ceram. Soc. (in press).
27. F. Deuerler, R. Knehan, and R. Steinbrech, in *Science of Ceramics 13*, Journal de Physique, Paris (1986), pp. C1-617–621.
28. P. L. Swanson, C. J. Fairbanks, B. R. Lawn, Y.-W. Mai, and B. J. Hockey, J. Am. Ceram. Soc. **70**, 279–289 (1987).
29. P. L. Swanson, in *Fractography of Glasses and Ceramics* (The American Ceramic Society, Westerville, OH, 1988), Vol. 22, pp. 135–155.
30. E. K. Beauchamp and S. L. Monroe, J. Am. Ceram. Soc. **72**, 1179–1184 (1989).
31. P. F. Becher, J. Am. Ceram. Soc. **74**, 255–269 (1991).
32. F. Guiberteau, N. P. Padture, H. Cai, and B. R. Lawn, Philos. Mag. A **68**, 1003–1016 (1993).
33. F. Guiberteau, N. P. Padture, and B. R. Lawn, J. Am. Ceram. Soc. (in press).
34. P. W. McMillan, *Glass-Ceramics* (Academic Press, London, 1979).
35. C. K. Chyung, G. H. Beall, and D. G. Grossman, in *Electron Microscopy and Structure of Materials*, edited by G. Thomas, R. M. Fulrath, and R. M. Fisher (University of California Press, Berkeley, CA, 1972), pp. 1167–1194.
36. K. Chyung, G. H. Beall, and D. G. Grossman, in *Proceedings of 10th International Glass Congress, No. 14* (The Ceramic Society of Japan, Tokyo, Japan, 1974), pp. 33–40.
37. K. Chyung, in *Fracture Mechanics of Ceramics*, edited by R. C. Bradt, D. P. H. Hasselman, and F. F. Lange (Plenum Press, New York, 1974), Vol. 2, pp. 495–508.
38. G. H. Beall, in *Advances in Nucleation and Crystallization in Glasses*, edited by L. L. Hench and S. W. Freiman (The American Ceramic Society, Westerville, OH, 1972), pp. 251–261.
39. T. Uno, T. Kasuga, and K. Nakajima, J. Am. Ceram. Soc. **74**, 3139–3141 (1991).

40. D. G. Grossman, in *Proceedings of the International Symposium on Computer Restorations*, edited by W. H. Mörmann (Quintessence Publishing Co., Chicago, IL, 1991), pp. 103–115.
41. C. J. Fairbanks, B. R. Lawn, R. F. Cook, and Y-W. Mai, in *Fracture Mechanics of Ceramics*, edited by R. C. Bradt, A. G. Evans, D. P. H. Hasselman, and F. F. Lange (Plenum, New York, 1986), Vol. 8, pp. 23–37.
42. T. O. Mulhearn, *J. Mech. Phys. Solids* **7**, 85–96 (1959).
43. R. F. Cook, B. R. Lawn, and C. J. Fairbanks, *J. Am. Ceram. Soc.* **68**, 604–615 (1985).
44. D. Tabor, *Hardness of Metals* (Clarendon, Oxford, 1951).
45. K. L. Johnson, *Contact Mechanics* (Cambridge University Press, London, 1985).
46. J. J. Benbow, *Proc. Phys. Soc. London* **75**, 697–699 (1960).
47. J. S. Williams, B. R. Lawn, and M. V. Swain, *Phys. Status Solidi A* **2**, 7–29 (1970).
48. J. C. Jaeger and N. G. W. Cook, *Fundamentals of Rock Mechanics* (Chapman and Hall, London, 1971).
49. M. S. Paterson, *Experimental Rock Deformation—The Brittle Field* (Springer-Verlag, Berlin, 1978).
50. R. L. Kranz, *Tectonophysics* **100**, 449–480 (1983).
51. L. R. Myer, J. M. Kemeny, Z. Zheng, R. Suarez, R. T. Ewy, and N. G. W. Cook, *Appl. Mech. Rev.* **45**, 263–280 (1992).
52. S. van der Zwagg, J. T. Hagan, and J. E. Field, *J. Mater. Sci.* **15**, 2965–2972 (1980).
53. K-T. Wan, N. Aimard, S. Lathabai, R. G. Horn, and B. R. Lawn, *J. Mater. Res.* **5**, 172–182 (1990).
54. K-T. Wan and B. R. Lawn, *Acta Metall.* **38**, 2073–2083 (1990).
55. K-T. Wan, D. T. Smith, and B. R. Lawn, *J. Am. Ceram. Soc.* **75**, 667–676 (1992).
56. H. Horii and S. Namat-Nasser, *J. Geophys. Res.* **90**, 3105–3125 (1985).
57. M. F. Ashby and S. D. Hallam, *Acta Metall. Mater.* **34**, 497–510 (1986).
58. B. R. Lawn, N. P. Padture, F. Guiberteau, and H. Cai, *Acta Metall.* (in press).
59. B. R. Lawn, N. P. Padture, L. M. Braun, and S. J. Bennison, *J. Am. Ceram. Soc.* **76**, 2235–2240 (1993).
60. N. P. Padture, J. L. Runyan, S. J. Bennison, L. M. Braun, and B. R. Lawn, *J. Am. Ceram. Soc.* **76**, 2241–2247 (1993).
61. H. Cai, M. A. Stevens Kalceff, and B. R. Lawn, *J. Mater. Res.* (unpublished research).
62. S. Lathabai, J. Rödel, and B. R. Lawn, *J. Am. Ceram. Soc.* **74**, 1340–1348 (1991).